Influence of interstitial cluster families on post-synthesis defect manipulation and purification of oxides using submerged surfaces \odot

Heonjae Jeong [⊚] ; Edmund G. Seebauer **≥** [©]



J. Chem. Phys. 161, 121103 (2024) https://doi.org/10.1063/5.0230224





Articles You May Be Interested In

Facile purification of $CsPbX_3$ (X = C I - , B r - , I -) perovskite nanocrystals

J. Chem. Phys. (September 2019)

Self-purification construction of interstitial O in the neighbor of Eu³⁺ ions to act as energy transfer bridge

Appl. Phys. Lett. (January 2014)

Communication: Generalized canonical purification for density matrix minimization

J. Chem. Phys. (March 2016)







Influence of interstitial cluster families on post-synthesis defect manipulation and purification of oxides using submerged surfaces •

Cite as: J. Chem. Phys. 161, 121103 (2024); doi: 10.1063/5.0230224 Submitted: 22 July 2024 · Accepted: 8 September 2024 · **Published Online: 25 September 2024**









Heonjae Jeong^{1,a)} o and Edmund G. Seebauer^{2,b)}



AFFILIATIONS

- Department of Mechanical Science and Engineering, University of Illinois at Urbana-Champaign, Urbana, Illinois 61801, USA
- ²Department of Chemical and Biomolecular Engineering, University of Illinois at Urbana-Champaign, Urbana, Illinois 61801, USA
- ^{a)} Present address: Department of Electronic Engineering, Gachon University, 1342 Seongnam-daero, Seongnam, Gyeonggi 13120, South Korea.
- b) Author to whom correspondence should be addressed: eseebaue@illinois.edu

ABSTRACT

Injection of interstitial atoms by specially prepared surfaces submerged in liquid water near room temperature offers an attractive approach for post-synthesis defect manipulation and isotopic purification in device structures. However, this approach can be limited by trapping reactions that form small defect clusters. The compositions and dissociation barriers of such clusters remain mostly unknown. This communication seeks to address this gap by measuring the dissociation energies of oxygen interstitial traps in rutile TiO2 and wurtzite ZnO exposed to liquid water. Isotopic self-diffusion measurements using ¹⁸O, combined with progressive annealing protocols, suggest the traps are small interstitial clusters with dissociation energies ranging from 1.3 to 1.9 eV. These clusters may comprise a family incorporating various numbers, compositions, and configurations of O and H atoms; however, in TiO2, native interstitial clusters left over from initial synthesis may also play a role. Families of small clusters are probably common in semiconducting oxides and have several consequences for post-synthesis defect manipulation and purification of semiconductors using submerged surfaces.

Published under an exclusive license by AIP Publishing. https://doi.org/10.1063/5.0230224

I. INTRODUCTION

Injection of interstitial atoms into semiconducting oxides by specially prepared surfaces submerged in liquid water near room temperature offers an attractive approach 1-3 for post-synthesis manipulation of atomic-scale defects and isotopic purification in device structures. In binary oxides, for example, injection of oxygen interstitials (Oi) eliminates O vacancies and helps neutralize unintentional donors, ^{4,5} including adventitious hydrogen. ^{6–10} Existing methods for defect control usually involve high temperatures that generate undesirable defects, 15 induce phase changes, and degrade nanostructures. Fast injection has the added benefit of generating steep interstitial gradients, which couple with statistical differences³ in the effective diffusivities of majority and minority isotopes to yield efficient isotopic fractionation. 16

The promise of surface interstitial injection can be limited by trapping reactions that form small defect clusters. 17,18 Such trapping restricts the penetration depth and steepens the nearsurface concentration gradient of interstitials, complicating and possibly restricting both defect manipulation and isotopic fractionation.¹⁹ Control of interstitial cluster dissociation through careful selection of annealing protocol has long been employed to optimize doping in silicon by ion implantation. 20-24 However, most defect clusters that are generated this way contain many atoms that are strongly bonded. Therefore, the clusters require high temperatures to dissociate. By contrast, interstitial injection into metal oxides near room temperature creates mainly small clusters. For example, small clusters can form in TiO2,3, $ZnO_{2}^{26,27}$ SnO_{2}^{28} $In_{2}O_{3}^{28,29}$ HfO_{2}^{30} $Ga_{2}O_{3}^{31-33}$ and $UO_{2}^{34,35}$ Such clusters seem to be less strongly bonded; however, the

possible compositions and dissociation barriers remain mostly unknown.

This communication seeks to address this gap by measuring the dissociation energies of O_i clusters in rutile TiO_2 and wurtzite ZnO immersed in liquid water. Isotopic self-diffusion measurements using ^{18}O , combined with isochronal annealing protocols at progressively increasing temperatures, suggest that the main traps for O_i are interstitial clusters with dissociation energies ranging from 1.3 to 1.9 eV. These clusters may comprise a family incorporating various numbers, compositions and configurations of O and H atoms, although in TiO_2 , native interstitial clusters left over from initial synthesis may also play a role.

II. EXPERIMENT

Isotopic self-diffusion experiments monitor the behavior of defects indirectly, as the concentration of atoms within defects lies below the detection technique limit of the chief analytic technique employed here: secondary ion mass spectrometry (SIMS). In this work, specially cleaned oxide specimens were submerged in water containing excess $^{18}\mathrm{O}$ as a label (10%) according to procedures described previously. 3,16,36,37 $^{18}\mathrm{O}$ enters the solid via injection of $\mathrm{O_{i}}$, 3 which then undergoes interstitial-mediated diffusion. Exchange of atoms between diffusing $\mathrm{O_{i}}$ and the lattice enables $^{18}\mathrm{O}$ to enter the lattice. Trapping reactions impede the diffusion of interstitials. 19 Depth profiles of $^{18}\mathrm{O}$ measured by SIMS after water exposure reflect the integrated history of $\mathrm{O_{i}}$ diffusion and trapping. Heating in air after the establishment of the initial $^{18}\mathrm{O}$ profile liberates trapped $\mathrm{O_{i}}$, which induces renewed profile spreading that is monitored with SIMS. Stages of heating at progressively higher temperatures induce the dissociation of clusters having correspondingly increasing barriers.

Experiments employed single-crystal specimens of rutile $TiO_2(110)$ (MTI Corp.) and wurtzite Zn-term ZnO(0001) (CrysTec GmbH), with procedures for submerged diffusion largely following those described previously. 3,16,36,37 Surfaces exhibited roughness <0.5 nm on the polished side as measured by atomic force microscopy. Specimens of thickness 0.5 mm were cut to dimensions of 5 × 10 mm² and degreased. To eliminate possible complications from O vacancies left by initial synthesis, specimens were annealed in natural-abundance O_2 in an ultrahigh vacuum-compatible chamber for 4 h at 500 °C and 1.0×10^{-5} Torr for ZnO and at 450 °C and 5.0×10^{-6} Torr for TiO₂.

Self-diffusion experiments employed a custom-designed apparatus for immersion in 18 O-labeled water (10 at.% 18 O, Sigma-Aldrich). Immersion lasted 1 h from 30 to 80 °C. The resulting 18 O concentration vs depth was measured *ex-situ* by SIMS (PHI-TRIFT III) using a Cs ion source (3 keV) for depth profiling. The spot diameter was about 0.5 mm. Surface charging due to incident ions was compensated by electron flooding. 18 O concentrations were calibrated according to the known natural abundance concentration (0.2%) in as-received specimens. Two to five profiles were measured at different locations on each specimen and were averaged. Stages of heating to temperatures T for 1 h in air employed a tube furnace (Thermolyne). The progression of T typically encompassed a range between 120 and 280 °C. Details of the progression for each specimen appear in Tables S1 and S2 in the supplementary

material. The upper temperature was set by the fact that, in most cases, the profiles decayed away entirely by 280 °C.

III. RESULTS

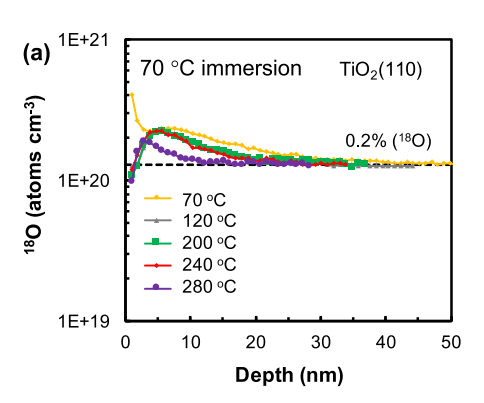
Figures 1 and 2, respectively, show example ^{18}O concentration profiles from progressive annealing sequences for TiO_2 and ZnO. Additional examples appear in Figs. S1 and S2 in the supplementary material. All specimens exhibit continual profile decay as T increases.

Dissociation energies were determined assuming first-order profile decay for all depths. In other words, the "excess" $^{18}\mathrm{O}$ concentration C above the natural-abundance baseline was assumed to decay exponentially from C_1 to C_2 during an increment of annealing time (t) according to

$$C_2/C_1 = \exp(-k(T)t).$$
 (1)

The dissociation rate constant k obeys a thermally activated expression,

$$k = k_0 \exp(-E/k_BT), \tag{2}$$



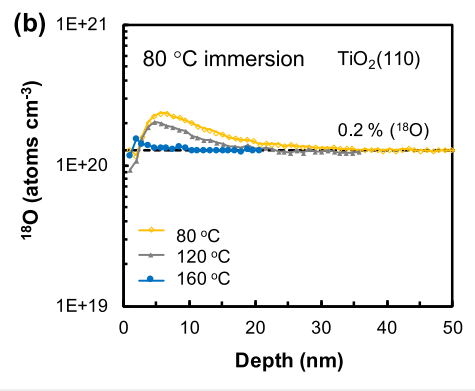
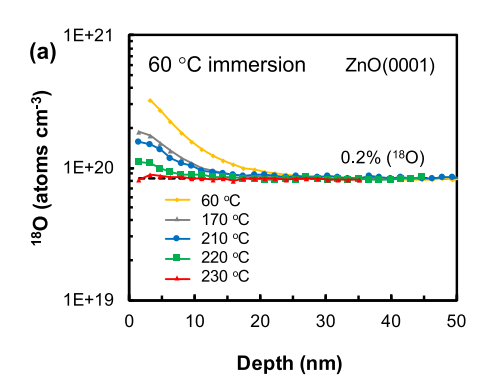


FIG. 1. Representative ^{18}O profiles for different TiO₂ specimens after various stages of progressive annealing. The yellow curves show profiles after exposure for 1 h to liquid H₂ ^{18}O at (a) 70 °C and (b) 80 °C but with no further annealing. Significant differences in profile evolution upon annealing are evident between (a) and (b). In (a), portions of the initial profile remain visible at 280 °C. In contrast, the above-baseline ^{18}O in (b) has vanished almost entirely by 160 °C. In (a), the profile at 120 °C (gray, not readily visible) overlaps with those at 200 and 240 °C, indicating that the ^{18}O does not evolve from 120 to 240 °C.



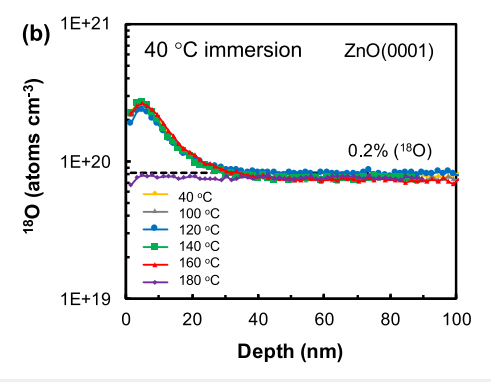


FIG. 2. Representative ¹⁸O profiles for different ZnO specimens after various stages of progressive annealing. The yellow curves [not readily visible in (b)] show profiles after exposure for 1 h to liquid $\rm H_2^{18}O$ at (a) 60 °C and (b) 40 °C but with no further annealing. Significant differences in profile evolution upon annealing are evident between (a) and (b). In (a), portions of the initial profile remain visible at 220 °C. In contrast, the above-baseline ¹⁸O in (b) has vanished almost entirely by 180 °C. In (b), the profiles at 40 and 100 °C (gray, not readily visible) overlap with those at 120, 140, and 160 °C, indicating that the ¹⁸O does not evolve from 40 to 160 °C.

where k_0 denotes the pre-exponential factor, assumed to be roughly the Debye frequency. E denotes the effective dissociation energy at T, and $k_{\rm B}$ is the Boltzmann constant.

Values of E for each temperature stage were determined by application of Eq. (1) at up to four different depths (4.8, 9.6, 14.4, and 19.2 nm) to yield a value of k at each depth. Figure 3 depicts the basic concept. In the near-surface region (<5 nm) of TiO_2 , profiles often exhibited non-monotonic shapes originating from isotopic fractionation. ¹⁶ Although fractionation is of technological interest, its behavior is complicated. Hence, sampling of concentration data avoided this region to simplify mathematical analysis. Application of Eq. (2) with the assumption of $k_0 = 10^{13} \, \rm s^{-1}$ yielded corresponding effective values of E, which were typically averaged over the four depths to yield a single aggregated value. Profile points lying too close to the baseline (i.e., where C started to approach the SIMS noise level) were excluded from the computation.

Figure 4 shows derived values of the cluster dissociation energy E as a function of T for TiO_2 and ZnO. Many energies are represented, ranging between about 1.3 and 1.9 eV. The origins of this range will be discussed below.

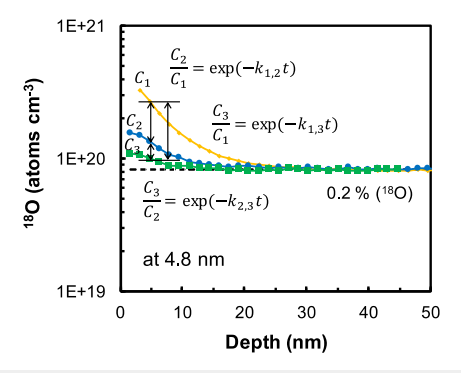


FIG. 3. Diagram illustrating how rate constants k(T) were calculated from measured ¹⁸O profiles in two successive cycles of progressive annealing. In this instance for ZnO diffused at 60 °C, concentrations C_1 and C_2 at the beginning and end of the first cycle at 210 °C were measured at a depth of 4.8 nm, with a third concentration C_3 measured after a second cycle at 220 °C. Concentrations were computed in terms of the additional ¹⁸O above the baseline concentration shown by the dashed line. Annealing time t was 1 h for both cycles. For a given cycle, determinations of k(T) at several depths were averaged to improve accuracy.

SIMS profiles varied slightly at different points on a given specimen due to adventitious poisoning of surface sites during both submerged diffusion and progressive annealing. During submerged diffusion, surface sites act as interstitial sources that can be poisoned

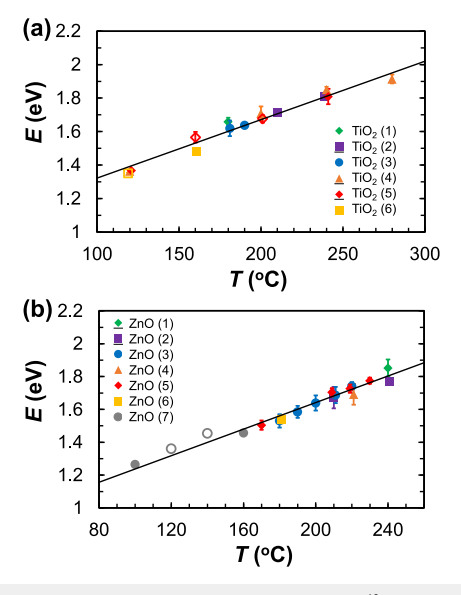


FIG. 4. Dissociation barrier energy E of labeled oxygen ¹⁸O of several (a) TiO₂ and (b) ZnO specimens. Error bars represent the random errors associated with profile-to-profile variations across the face of a given specimen, and in some cases are invisible because the spacing falls below the width of a data symbol. Open symbols indicate that no dissociation occurred during the immediately preceding progressive annealing step. The coexistence of solid and open symbols at numerous temperatures reflects the variability among specimens. The underbar for several symbols in the legend indicates the corresponding profiles did not fully disappear even at the highest temperatures to which those specimens were subjected. Lines represent least squares fits. Numbers in parentheses signify different specimens detailed in the supplementary material.

on both TiO₂³⁸ and ZnO.³⁹ The most likely poison is adventitious carbon, which inhibits the dissociation of adsorbed OH into O and H, elementary-step injection of O_i, or both.³⁶ This poisoning propagates into localized variations in the injected flux, typically by a factor of two.³⁶ Depending upon the propensity of traps to saturate, such variations may affect the shape of the distribution function for E (concentration of sites vs E) but probably have minimal effect on the values of E represented.

During progressive annealing, dissociating clusters act as interstitial sources, and the surface becomes a sink. Complete elimination of a label profile requires about as many interstitials from dissociation as the formation of the profile requires during injection. In other words, profile disappearance corresponds to essentially complete liberation of trapped interstitials. Annihilation represents the kinetic inverse of injection and is subject to poisoning as well,40 although in air no aqueous chemistry is involved. A high annihilation probability efficiently removes interstitials from the solid, and thereby attenuates diffusional spreading. Clusters present in small concentrations release only a few interstitials to begin with; thus, a high annihilation probability makes such clusters more difficult to detect. Spatial variations in annihilation probability translate into variations in sensitivity to low-concentration clusters. Fortunately, such effects do not distort E for clusters sufficiently concentrated to

Uncertainties in E arose from several sources. Measurements at different depths led to variations in the value of C_i/C_{i-1} although the resulting values of k were averaged to reduce the effects. Moreover, larger temperature increments act to average the dissociation energies over larger ranges of the energy distribution and lead to slightly different values for E. The temperature increments often varied from specimen to specimen, which propagated into E. All these effects gave rise to error bars in E averaging ± 0.17 eV for TiO₂ and ± 0.14 eV for ZnO.

Figure 4 shows several points with open symbols, which represent annealing stages manifesting no measurable profile spreading. Such stages still contain useful information, as the E can still be estimated with considerable accuracy as follows. For constant t = 1 h, the magnitude of k varies within a rather narrow range set by the values of C_i/C_{i-1} that are useable in Eq. (1). Given the modest temperature increments employed, this ratio typically varied between 0.7 and 1, with an average of about 0.9 for most data in TiO2. For ZnO, that ratio varied more broadly between 0.4 and 1.0, with an average of about 0.7. This latter number, together with the assumed pre-exponential factor and Eq. (2), leads to a line having a slope of about 3.4×10^{-3} eV/K that enables estimation of E.

IV. DISCUSSION

The significance of Fig. 4 does not rest upon the linear functional form that relates E and T, the value of the slope, or the fact that all points fall near the line. These features follow straightforwardly from the estimation method just outlined. The significance of Fig. 4 is rather that (1) the range of points represented is fairly wide at ~ 0.6 eV, (2) the general magnitude of E averages roughly 1.6 eV, (3) the energies are similar for the two oxides, and (4) gaps in the distribution imply distribution functions with complicated shapes.

The large range of energies represented in Fig. 4 implies the existence of traps for Oi in both TiO2 and ZnO having rather

broad distributions of dissociation energies. This behavior mirrors that observed in many solid systems wherein chemically bonded species reside not in one energy state E, but rather in one or more groups of closely spaced states. ⁴¹ An example is gases adsorbed on polycrystalline surfaces or small particles that expose many crystal faces. $^{42-44}$ The average of E matches that average inferred 36 for ZnO from self-diffusion measurements at much higher temperatures with gaseous O2 as the fluid. The close correspondence is remarkable given the differing conditions and modeling approaches. Small interstitial clusters were hypothesized to dominate O_i trapping in that work as well, although a T-dependent trap concentration was required to satisfactorily reproduce the experimental profiles. For corresponding high-T gas measurements in TiO₂, where slowly ripening extended defects appear to dominate Oi trapping, the characteristic trap dissociation energy is much higher at 3.3 eV.²

Determination of the distribution function from measurements of dissociation rates is challenging because the problem is mathematically ill-conditioned and sensitive to small variations in the data. 42,43,45 As a result, this work did not attempt to measure the distribution function itself but only the energies represented within that distribution. However, the existence of gaps in *E* for some specimens of both ZnO and TiO₂ shows that the distributions have complicated shapes—not simple like a Gaussian distribution, for example.

Interstitial atoms in semiconductors commonly exhibit a strong tendency to cluster together, sometimes in families of clusters having varying sizes and closely related compositions. In Si, for example, a family of self-interstitial (Si_i) clusters ranges in size from dimers to hundreds of atoms, with corresponding dissociation energies ranging between 3.1 and 4.0 eV.46 An analogous family of mixed-composition Si_i-B clusters exhibits a similar range of dissociation energies.4

Which elements compose the family (or families) of small clusters responsible for the energy spread in Fig. 4? Chemical reasoning offers important clues. By analogy with the behavior of Si, a natural candidate is dimers or higher order clusters consisting entirely of O_i. Such clusters exist in UO₂,³⁵ but UO₂ represents an unusual oxide wherein the metal cation and O anion have comparable ionic radii (typically near 103 and 126 pm, respectively, with variations depending upon coordination number). This similarity in ionic radii enables Oi cluster formation without straining the lattice excessively. In TiO₂ and ZnO, however, the respective cations have much smaller radii, typically near 74 and 88 pm. Clustering of multiple Oi atoms imposes more strain and the lattice and is less energetically stable. Thus, it seems unlikely that a large family of O_i clusters could give rise to the wide, nearly continuous distribution indicated in Fig. 4.

Another possible family could include mixed clusters of O_i and self-interstitials of the host cations: Ti_i or Zn_i. However, the cation interstitials in both oxides have hopping barriers below 0.6 eV, which makes them too mobile at the temperatures employed here to exist freely as traps for diffusing Oi. Shortly after initial crystal synthesis, the cation interstitials will have become trapped themselves at surfaces, extended defects, or other locations within the crystal. Therefore, no mechanism exists to nucleate mixed interstitial

A different possibility could involve small native interstitial clusters left over in the near-surface region from cutting and polishing of the crystal surfaces during initial manufacturing. In this work, presumably, some of these clusters would have disappeared during annealing in O2 at 450-500 °C before submerged diffusion, which injects O_i to remove O vacancies^{3,16,36} and simultaneously removes cation interstitials by surface annihilation, at least in TiO25 and possibly in ZnO. In ZnO, the similarity in the average value of E in gas and liquid self-diffusion experiments argues against a special role for vestigial near-surface clusters, as the gas experiments sample the bulk to a depth on the order of 10⁵ nm. The similarity between ZnO and TiO₂ in the range and average of E suggests similarity in the trapping mechanisms but does not constitute proof. Hence, the evidence for ruling out a role for vestigial near-surface mixed clusters is not as strong for TiO_2 as for ZnO.

Another possible family could include mixed clusters of O_i and cation vacancies (V): $\dot{V}_{Ti}^{53,54}$ or $V_{Zn}.^{51}$ These vacancies have lower formation energies in n-type material than the corresponding interstitials under O-rich conditions near room temperature, so cation vacancies could exist as free species for trapping O_i. However, V_{Ti} and V_{Zn} act as strong acceptors (-4 charge state), which seem unlikely to react extensively with Oi that also has acceptor tendencies, especially in TiO2. The same characteristic likely precludes the formation of mixed vacancy-Oi clusters left over from cutting and polishing.

A likely candidate that contributes to Fig. 4 includes clusters with hydrogen as a key constituent. H is present in essentially all oxides 10 and exists in several forms, including interstitially as Hi, substitutionally (for lattice O) as H_O, and in molecular form as H₂. H_i bonds with numerous interstitial, vacancy, and substitutional defects. Many such clusters incorporate more than one H and, thus, form families. In ZnO, for example, multiple H atoms form clusters with Zn vacancies²⁷ and with the complex of substitutional N and V_{Zn}.⁵⁵ In Si, substitutional B^{56,57} forms clusters with one or two H. Up to four H can cluster with Si self-interstitials,⁵⁶ H is believed to decorate interstitial defects involving O and C.60 In UO2, varying numbers of H stabilize Willis clusters, which comprise a family of O_i-based clusters of assorted sizes.³⁴ In TiO₂ and ZnO, O_i-H_i has been shown by DFT (density functional theory) calculations to exist stably with a low formation barrier.3 Thus, it is reasonable to suppose that a family of interstitial clusters containing both O_i and H_i exists in both TiO₂ and ZnO.

However, akin to Ti_i and Zn_i, H_i has significant diffusional mobility in both TiO2 and ZnO at the temperatures examined here. 9,27,61,62 That mobility, together with the strong propensity of H_i to react, suggests that no free H_i exists in the solid as O_i injection begins. However, DFT simulations have shown that H_0 in rutile^{63,6} acts as a shallow donor-a result confirmed experimentally. 65,66 Thus, acceptor O_i seems likely to react with donor Ho via kick-out to yield lattice O and Hi. The latter would then react with O_i or existing clusters to build a family.

Oi may also react with molecular H2 caged within the solid structure. H₂ is known to exist in ZnO.⁶⁷ The H₂ resides at interstitial sites and O vacancy agglomerates. It dissociates below 700 °C – a modest temperature compared to the gas phase. Although H₂ has not been reported within rutile, several other metal oxides host this species⁶⁸ including anatase TiO₂ where the formation of H₂ is 0.2 eV more stable than two separated H_i.⁶⁹ H₂ dissociates at an O vacancy into two neighboring but separated atoms⁷⁰ – suggesting a strong generic propensity to react. H₂ may plausibly react with

O_i to form O_i-H_i and free H_i, which itself goes on to react with a

Regardless of which species causes the behavior in Fig. 4, the plots clearly demonstrate that such families exist for two common oxides. It is reasonable to suppose such families exist in other oxides, with several significant consequences for post-synthesis defect manipulation and purification of semiconductors using submerged surfaces. First, families multiply the pathways by which injecting interstitials may be trapped, thereby raising the quantity of injecting interstitials required to saturate and bypass the traps for deep penetration into the solid. Second, families with wide and quasi-continuous distributions of dissociation energies increase the likelihood that weakly bonded members will dissociate slowly after injection ends. Thus, important physical properties of the solid (e.g., donor concentration) may drift over time, especially if the material experiences slight heating during use. Eliminating such drift might be avoided by using higher temperatures during injection. A better approach would entail a separate warming step after injection in the presence of a surface with high annihilation probability. Third, nonthermal means to destabilize clusters, such as super-bandgap illumination,³⁷ could be complicated by large disparities among family members in the interaction with photogenerated charge carriers. Behavior would be dominated by those clusters having the largest cross section for carrier capture.

V. CONCLUSION

Isotopic self-diffusion measurements using ¹⁸O in rutile TiO₂ and wurtzite ZnO, combined with progressive annealing protocols, have uncovered Oi traps with dissociation energies ranging from 1.3 to 1.9 eV. These traps are likely to involve a family of small interstitial clusters comprising O and H atoms in various numbers, compositions, and configurations; however, in TiO2, native interstitial clusters left over from initial synthesis may also play a role. Families of small clusters are probably common in semiconducting oxides and have several consequences for post-synthesis defect manipulation and purification of semiconductors using submerged surfaces. Small-cluster families raise the quantity of injecting interstitials required for trap saturation, may necessitate a separate warming step to prevent material property drift, and may complicate the use of photostimulation to promote cluster dissociation.

SUPPLEMENTARY MATERIAL

See the supplementary material for detailed descriptions of progressive annealing protocols for each specimen and for additional plots of ¹⁸O profiles.

ACKNOWLEDGMENTS

This work was supported by the U.S. National Science Foundation (Grant Nos. DMR 17-09327 and DMR 23-22121) and the Air Force Office of Scientific Research (Grant No. FA9550-21-1-0353). SIMS measurements were performed in the Materials Research Laboratory Central Research Facilities, University of Illinois at Urbana-Champaign. The authors thanked Dr. Ian I. Suni for helpful comments on the manuscript.

AUTHOR DECLARATIONS

Conflict of Interest

The authors have no conflicts to disclose.

Author Contributions

Heonjae Jeong: Formal analysis (equal); Investigation (equal); Writing – review & editing (supporting). **Edmund G. Seebauer**: Conceptualization (lead); Writing – original draft (lead); Writing – review & editing (lead).

DATA AVAILABILITY

The data that support the findings of this study are available within the article and its supplementary material.

REFERENCES

- ¹H. Jeong, M. Li, J. Kuang, E. Ertekin, and E. G. Seebauer, "Mechanism of creation and destruction of oxygen interstitial atoms by nonpolar zinc oxide(1010) surfaces," Phys. Chem. Chem. Phys. 23, 16423–16435 (2021).
- ²H. Jeong, E. Ertekin, and E. G. Seebauer, "Kinetic control of oxygen interstitial interaction with TiO₂(110) via the surface Fermi energy," Langmuir **36**(42), 12632–12648 (2020).
- ³H. Jeong, E. Ertekin, and E. G. Seebauer, "Surface-based post-synthesis manipulation of point defects in metal oxides using liquid water," ACS Appl. Mater. Interfaces 14(29), 34059–34068 (2022).
- ⁴A. Bikowski, T. Welzel, and K. Ellmer, "The impact of negative oxygen ion bombardment on electronic and structural properties of magnetron sputtered ZnO:Al films," Appl. Phys. Lett. **102**(24), 242106 (2013).
- ⁵K. Ellmer and A. Bikowski, "Intrinsic and extrinsic doping of ZnO and ZnO alloys," J. Phys. D Appl. Phys. **49**(41), 413002 (2016).
- ⁶A. Janotti and C. G. Van de Walle, "Hydrogen multicentre bonds," Nat. Mater. **6**(1), 44–47 (2007).
- ⁷H. Li and J. Robertson, "Behaviour of hydrogen in wide band gap oxides," J. Appl. Phys. **115**(20), 203708 (2014).
- ⁸ A. Venzie, A. Portoff, E. C. P. Valenzuela, M. Stavola, W. B. Fowler, S. J. Pearton, and E. R. Glaser, "Impurity-hydrogen complexes in β -Ga₂O₃: Hydrogenation of shallow donors vs deep acceptors," J. Appl. Phys. **131**(3), 035706 (2022).
- ⁹A. J. Hupfer, E. V. Monakhov, B. G. Svensson, I. Chaplygin, and E. V. Lavrov, "Hydrogen motion in rutile TiO₂," Sci. Rep. 7(1), 17065 (2017).
- ¹⁰ M. D. McCluskey, M. C. Tarun, and S. T. Teklemichael, "Hydrogen in oxide semiconductors," J. Mater. Res. 27(17), 2190–2198 (2012).
- ¹¹T. Sinno, E. Dornberger, W. von Ammon, R. A. Brown, and F. Dupret, "Defect engineering of Czochralski single-crystal silicon," Mater. Sci. Eng.: R: Rep. **28**(5-6), 149–198 (2000).
- ¹²M. Canino, G. Regula, M. Xu, E. Ntzoenzok, and B. Pichaud, "Defect engineering via ion implantation to control B diffusion in Si," Mater. Sci. Eng.: B 159–160, 338–341 (2009).
- ¹³H. L. Tuller and S. R. Bishop, "Point defects in oxides: Tailoring materials through defect engineering," Annu. Rev. Mater. Res. 41(1), 369–398 (2011).
- ¹⁴J. S. Park, S. Kim, Z. Xie, and A. Walsh, "Point defect engineering in thin-film solar cells," Nat. Rev. Mater. 3(7), 194–210 (2018).
- ¹⁵L. Schmidt-Mende and J. L. MacManus-Driscoll, "ZnO—Nanostructures, defects, and devices," Mater. Today 10(5), 40–48 (2007).
- ¹⁶H. Jeong and E. G. Seebauer, "Strong isotopic fractionation of oxygen in TiO₂ obtained by surface-enhanced solid-state diffusion," J. Phys. Chem. Lett. 13, 9841–9847 (2022).
- ¹⁷J. K. Cooper, S. B. Scott, Y. Ling, J. Yang, S. Hao, Y. Li, F. M. Toma, M. Stutzmann, K. V. Lakshmi, and I. D. Sharp, "Role of hydrogen in defining the n-type character of BiVO₄ photoanodes," Chem. Mater. 28(16), 5761–5771 (2016).

- ¹⁸A. Lushchik, V. N. Kuzovkov, E. A. Kotomin, G. Prieditis, V. Seeman, E. Shablonin, E. Vasil'chenko, and A. I. Popov, "Evidence for the formation of two types of oxygen interstitials in neutron-irradiated α -Al₂O₃ single crystals," Sci. Rep. 11(1), 20909 (2021).
- ¹⁹Y. Knausgård Hommedal, M. Etzelmüller Bathen, V. Mari Reinertsen, K. Magnus Johansen, L. Vines, and Y. Kalmann Frodason, "Theoretical modeling of defect diffusion in wide bandgap semiconductors," J. Appl. Phys. 135(17), 170902 (2024)
- ²⁰N. E. Grant, F. E. Rougieux, and D. Macdonald, "Low temperature activation of grown-in defects limiting the lifetime of high purity n-type float-zone silicon wafers," in *Solid State Phenomena* (Trans Tech Publications, 2016), pp. 120–125.
- ²¹ N. E. Grant, V. P. Markevich, J. Mullins, A. R. Peaker, F. Rougieux, and D. Macdonald, "Thermal activation and deactivation of grown-in defects limiting the lifetime of float-zone silicon," Phys. Status Solidi RRL 10(6), 443–447 (2016).
- ²²N. E. Grant, V. P. Markevich, J. Mullins, A. R. Peaker, F. Rougieux, D. Macdonald, and J. D. Murphy, "Permanent annihilation of thermally activated defects which limit the lifetime of float-zone silicon," Phys. Status Solidi A 213(11), 2844–2849 (2016).
- ²³ J. Mullins, V. P. Markevich, M. Vaqueiro-Contreras, N. E. Grant, L. Jensen, J. Jabłoński, J. D. Murphy, M. P. Halsall, and A. R. Peaker, "Thermally activated defects in float zone silicon: Effect of nitrogen on the introduction of deep level states," J. Appl. Phys. 124(3), 35701 (2018).
- ²⁴D. Hiller, V. P. Markevich, J. A. T. de Guzman, D. König, S. Prucnal, W. Bock, J. Julin, A. R. Peaker, D. Macdonald, N. E. Grant, and J. D. Murphy, "Kinetics of bulk lifetime degradation in float-zone silicon: Fast activation and annihilation of grown-in defects and the role of hydrogen versus light," Phys. Status Solidi A 217(17), 2000436 (2020).
- $^{\mathbf{25}}$ G. Bromiley, N. Hilaret, and C. McCammon, "Solubility of hydrogen and ferric iron in rutile and TiO₂ (II): Implications for phase assemblages during ultrahighpressure metamorphism and for the stability of silica polymorphs in the lower mantle," Geophys. Res. Lett. **31**(4), L04610, https://doi.org/10.1029/2004gl019430 (2004).
- ²⁶Y. K. Frodason, K. M. Johansen, T. S. Bjørheim, B. G. Svensson, and A. Alkauskas, "Zn vacancy-donor impurity complexes in ZnO," Phys. Rev. B **97**(10), 104109 (2018).
- ²⁷M. D. McCluskey, "1—Defects in ZnO," in *Defects in Advanced Electronic Materials and Novel Low Dimensional Structures*, edited by J. Stehr, I. Buyanova, and W. Chen (Woodhead Publishing, 2018), pp. 1–25.
- $^{\mathbf{28}}$ I. Makkonen, E. Korhonen, V. Prozheeva, and F. Tuomisto, "Identification of vacancy defect complexes in transparent semiconducting oxides ZnO, In_2O_3 and SnO_2 ," J. Phys.: Condens. Matter $\mathbf{28}(22), 224002 \ (2016).$
- ²⁹E. Korhonen, F. Tuomisto, O. Bierwagen, J. S. Speck, and Z. Galazka, "Compensating vacancy defects in Sn- and Mg-doped In₂O₃," Phys. Rev. B **90**(24), 245307 (2014).
- ³⁰S. Kumar, S. B. Rai, and C. Rath, "Multifunctional role of dysprosium in HfO₂: Stabilization of the high temperature cubic phase, and magnetic and photoluminescence properties," Phys. Chem. Chem. Phys. **19**(29), 18957–18967 (2017).
- ³¹ J. M. Johnson, Z. Chen, J. B. Varley, C. M. Jackson, E. Farzana, Z. Zhang, A. R. Arehart, H. L. Huang, A. Genc, S. A. Ringel, C. G. Van De Walle, D. A. Muller, and J. Hwang, "Unusual Formation of point-defect complexes in the ultrawide-band-gap semiconductor β -Ga₂O₃," Phys Rev X **9**(4), 041027 (2019).
- ³² M. E. Ingebrigtsen, A. Y. Kuznetsov, B. G. Svensson, G. Alfieri, A. Mihaila, U. Badstübner, A. Perron, L. Vines, and J. B. Varley, "Impact of proton irradiation on conductivity and deep level defects in β-Ga₂O₃," APL Mater. **7**(2), 022510 (2019).
- ³³Y. K. Frodason, C. Zimmermann, E. F. Verhoeven, P. M. Weiser, L. Vines, and J. B. Varley, "Multistability of isolated and hydrogenated Ga–O divacancies in β -Ga₂O₃," Phys. Rev. Mater. 5(2), 025402 (2021).
- ³⁴J. M. Flitcroft, M. Molinari, N. A. Brincat, N. R. Williams, M. T. Storr, G. C. Allen, and S. C. Parker, "The critical role of hydrogen on the stability of oxyhydroxyl defect clusters in uranium oxide," J. Mater. Chem. A **6**(24), 11362–11369 (2018).
- ³⁵J. Wang, R. C. Ewing, and U. Becker, "Average structure and local configuration of excess oxygen in UO_{2+x}," Sci. Rep. 4(1), 4216 (2014).

- $^{36}\mathrm{H}.$ Jeong and E. G. Seebauer, "Effects of adventitious impurity adsorption on oxygen interstitial injection rates from submerged TiO₂(110) and ZnO(0001) surfaces," J. Vac. Sci. Technol., A **41**(3), 033203 (2023).
- $^{\bf 37}$ H. Jeong and E. G. Seebauer, "Effects of ultraviolet illumination on oxygen interstitial injection from TiO $_{\bf 2}$ under liquid water," J. Phys. Chem. C $\bf 126(49)$, 20800–20806 (2022).
- ³⁸ A. G. Hollister, P. Gorai, and E. G. Seebauer, "Surface-based manipulation of point defects in rutile TiO₂," Appl. Phys. Lett. **102**(23), 231601 (2013).
- ³⁹M. Li and E. G. Seebauer, "Surface-based control of oxygen interstitial injection into ZnO via submonolayer sulfur adsorption," J. Phys. Chem. C **120**(41), 23675–23682 (2016).
- ⁴⁰E. G. Seebauer, K. Dev, M. Y. L. Jung, R. Vaidyanathan, C. T. M. Kwok, J. W. Ager, E. E. Haller, and R. D. Braatz, "Control of defect concentrations within a semiconductor through adsorption," Phys. Rev. Lett. 97(5), 055503 (2006).
- ⁴¹S. Vyazovkin, A. K. Burnham, L. Favergeon, N. Koga, E. Moukhina, L. A. Pérez-Maqueda, and N. Sbirrazzuoli, "ICTAC Kinetics Committee recommendations for analysis of multi-step kinetics," Thermochim. Acta **689**, 178597 (2020).
- ⁴²E. G. Seebauer, "Quantitative extraction of continuous distributions of energy states and pre-exponential factors from thermal desorption spectra," Surf. Sci. 316(3), 391–405 (1994).
- ⁴³H. Wittkopf, "Calculation of desorption energy distribution applied to temperature programmed H₂O desorption from silicate glass surface: H Wittkopf, Vacuum 37, 1987, 819–823," Vacuum 39(5), 491 (1989).
- ⁴⁴P. J. Barrie, "Analysis of temperature programmed desorption (TPD) data for the characterisation of catalysts containing a distribution of adsorption sites," Phys. Chem. Chem. Phys. 10(12), 1688 (2008).
- ⁴⁵G. Carter, P. Bailey, D. G. Armour, and R. Collins, "The deduction of continuously distributed activation energy site populations from tempering schedules," Vacuum 32(5), 233–241 (1982).
- ⁴⁶N. E. B. Cowern, G. Mannino, P. A. Stolk, F. Roozeboom, H. G. A. Huizing, J. G. M. van Berkum, F. Cristiano, A. Claverie, and M. Jaraíz, "Cluster ripening and transient enhanced diffusion in silicon," Mater. Sci. Semicond. Process. 2(4), 369–376 (1999).
- ⁴⁷L. Pelaz, M. Jaraiz, G. H. Gilmer, H.-J. Gossmann, C. S. Rafferty, D. J. Eaglesham, and J. M. Poate, "B diffusion and clustering in ion implanted Si: The role of B cluster precursors," Appl. Phys. Lett. **70**(17), 2285–2287 (1997).
- ⁴⁸ M. Y. L. Jung, R. Gunawan, R. D. Braatz, and E. G. Seebauer, "A simplified picture for transient enhanced diffusion of boron in silicon," J. Electrochem. Soc. **151**(1), G1 (2003).
- ⁴⁹J. Schermer, A. Martinez-Limia, P. Pichler, C. Zechner, W. Lerch, and S. Paul, "On a computationally efficient approach to boron-interstitial clustering," Solid-State Electron. **52**(9), 1424–1429 (2008).
- ⁵⁰ K. L. Gilliard-AbdulAziz and E. G. Seebauer, "Microkinetic model for reaction and diffusion of titanium interstitial atoms near a TiO2(110) surface," Phys. Chem. Chem. Phys. 20(6), 4587–4596 (2018).
- ⁵¹A. Janotti and C. G. Van de Walle, "Fundamentals of zinc oxide as a semiconductor," Rep. Prog. Phys. **72**(12), 126501 (2009).

- ⁵² K. L. Gilliard and E. G. Seebauer, "Manipulation of native point defect behavior in rutile TiO₂ via surfaces and extended defects," J. Phys.: Condens. Matter 29(44), 445002 (2017).
- ⁵³ X. Li, M. W. Finnis, J. He, R. K. Behera, S. R. Phillpot, S. B. Sinnott, and E. C. Dickey, "Energetics of charged point defects in rutile TiO2 by density functional theory," Acta Mater. 57(19), 5882–5891 (2009).
- 54 H. Peng, "First-principles study of native defects in rutile TiO₂," Phys. Lett. A 372 (9), 1527–1530 (2008).
- ⁵⁵D. Y. Yong, H. Y. He, Z. K. Tang, S.-H. Wei, and B. C. Pan, "H-stabilized shallow acceptors in N-doped ZnO," Phys. Rev. B **92**(23), 235207 (2015).
- ⁵⁶C. P. Herrero, M. Stutzmann, and A. Breitschwerdt, "Boron-hydrogen complexes in crystalline silicon," Phys. Rev. B **43**(2), 1555–1575 (1991).
- 57 J. A. T. De Guzman, V. P. Markevich, J. Coutinho, N. V. Abrosimov, M. P. Halsall, and A. R. Peaker, "Electronic properties and structure of Boron-hydrogen complexes in crystalline silicon," Sol. RRL 6(5), 2100459 (2022).
- ⁵⁸M. Budde, B. Bech Nielsen, P. Leary, J. Goss, R. Jones, P. R. Briddon, S. Öberg, and S. J. Breuer, "Identification of the hydrogen-saturated self-interstitials in silicon and germanium," Phys. Rev. B **57**(8), 4397–4412 (1998).
- ⁵⁹B. Hourahine, R. Jones, S. Öberg, and P. R. Briddon, "Self-interstitial–hydrogen complexes in silicon," Phys. Rev. B **59**(24), 15729–15732 (1999).
- 60 A. Kiyoi, N. Kawabata, K. Nakamura, and Y. Fujiwara, "Influence of oxygen on trap-limited diffusion of hydrogen in proton-irradiated n -type silicon for power devices," J. Appl. Phys. **129**(2), 025701 (2021).
- ⁶¹O. W. Johnson, S. –H. Paek, and J. W. DeFord, "Diffusion of H and D in TiO₂: Suppression of internal fields by isotope exchange," J. Appl. Phys. **46**(3), 1026–1033 (1975).
- ⁶²M. A. Motin, P. C. Roy, and C. M. Kim, "The effect of the crystallographic orientation of ZnO on the surface adsorption and bulk diffusion of hydrogen," Phys. Status Solidi B 253(8), 1649–1652 (2016).
- ⁶³ L.-B. Mo, Y. Wang, Y. Bai, Q.-Y. Xiang, Q. Li, W.-Q. Yao, J.-O. Wang, K. Ibrahim, H.-H. Wang, C.-H. Wan, and J.-L. Cao, "Hydrogen impurity defects in rutile TiO₂," Sci. Rep. 5(1), 17634 (2015).
- ⁶⁴T. S. Bjørheim, S. Stølen, and T. Norby, "*Ab initio* studies of hydrogen and acceptor defects in rutile TiO₂," Phys. Chem. Chem. Phys. **12**(25), 6817–6825 (2010).
- ⁶⁵E. V. Lavrov, T. Mchedlidze, and F. Herklotz, "Photoconductive detection of hydrogen in ZnO and rutile TiO₂," J. Appl. Phys. **120**(5), 055703 (2016).
- ⁶⁶ J. Weber, E. V. Lavrov, and F. Herklotz, "Hydrogen shallow donors in ZnO and rutile TiO₂," Physica B **407**(10), 1456–1461 (2012).
- ⁶⁷S. G. Koch, E. V. Lavrov, and J. Weber, "Towards understanding the hydrogen molecule in ZnO," Phys. Rev. B **90**(20), 205212 (2014).
- ⁶⁸E. V. Lavrov, I. Chaplygin, F. Herklotz, V. V. Melnikov, and Y. Kutin, "Hydrogen in single-crystalline anatase TiO₂," J. Appl. Phys. **131**(3), 030902 (2022).
- ⁶⁹ E. V. Lavrov, I. Chaplygin, F. Herklotz, and V. V. Melnikov, "Hydrogen donors in anatase TiO₂," Phys. Status Solidi B 258(8), 2100171 (2021).
- ⁷⁰Y. Yang, L.-C. Yin, Y. Gong, P. Niu, J.-Q. Wang, L. Gu, X. Chen, G. Liu, L. Wang, and H.-M. Cheng, "An unusual strong visible-light absorption band in red anatase TiO₂ photocatalyst induced by atomic hydrogen-occupied oxygen vacancies," Adv. Mater. 30(6), 1704479 (2018).